A Practical Guide to Optical Trapping

Joshua W. Shaevitz
jshaevitz@berkeley.edu

August 22, 2006

1 Introduction to optical trapping

In the last few decades, novel microscopy techniques have been developed to monitor the activity of single enzymes as they perform their biological functions in vitro. Motor proteins such as kinesin, myosin, F_1F_o ATPase, and RNA polymerase have been mercilessly subjected to magnetic, elastic, and optical forces [14, 40, 48, 16, 18]. In 1986, Ashkin and colleagues reported the first observation of a stable three-dimensional optical trap, or optical tweezers, created using radiation pressure from a single laser beam [4]. Only a few years later, Block and colleagues had used an optical trap to manipulate and apply forces to *E. coli* flagella [8] and single kinesin motors [9]. Optical traps use light to manipulate microscopic objects as small as 10 nm using the radiation pressure from a focused laser beam. In addition, measurement of the light deflection yields information about the position of the object in the laser focus. Many excellent reviews have been written about optical trapping, its uses, and designs, see e.g. [2, 6, 22, 27, 37, 38, 43]. In particular, Lang and Block [23] is a thorough review of the optical trapping literature. This manuscript is meant to be a practical guide to understanding optical traps, and not an in depth review. When possible, simple examples and explanations are used to give the reader an intuitive feel for how these systems work and how they are implemented. I hope that this document will continue to improve, and welcome any comments.

The picoNewton and nanometer ranges of force and distance accessible to optical traps make them particularly useful for studying biological systems (Fig. 1) [7]. Optical forces have been used to investigate structural properties of biological polymers such as DNA [10, 46], membranes [39], whole cells [3] and microtubules [21]. Microrheological properties of these objects can be probed through the application of forces either to the object itself, or to a small dielectric sphere, or bead, to which the object is attached. Molecular motors represent the most used application of optical traps in the biological sciences. A great deal has been learned about kinesin [1, 9, 11, 12, 19, 20, 44], dynein [26, 25], myosin [28, 32, 33, 41, 42], and RNA polymerase [13, 15, 30, 36, 45] using optical forces.

2 How optical traps work

In the focus of a laser beam a dielectric particle, such as a glass or polystyrene bead, experiences a force, called the gradient force, that tends to bring push towards the laser focus where the light intensity is highest. This force arises from the momentum imparted to the bead as it scatters the laser light. Although the full theory of optical trapping is quite complex (see e.g. Rohrbach and Stelzer [34]), a few simplified examples allow for a good working intuition. The easiest case to consider occurs when the particle is much larger than the wavelength of light and is displaced from the laser focus laterally (Fig. 2A). When the particle sits to the right of the laser focus, f, the overall direction of propagation of the laser beam is deflected to the right. Rays a and b are refracted such that they meet to the right of the laser focus. The momentum change of these photons imparts an equal and opposite momentum

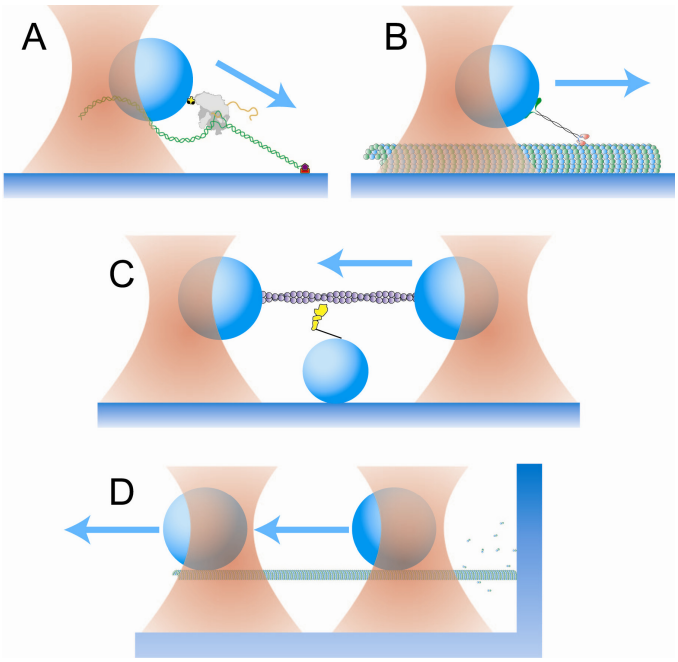

Figure 1: Different Optical Trapping Assays. (A) Optical trapping studies of RNA polymerase typically fix the polymerase to a optically trapped bead while the distal end of the DNA is attached to the microscope coverslip. As the polymerase moves along the DNA it must do work against the optical trap. (B) In a typical assay of kinesin motion, a motor–coated bead moves along a microtubule towards its plus–end, while being subjected to a retarding force by the optical trap. (C) Studies of non-processive motors, such as muscle myosin and NCD, often involve more complicated geometries and multiple optical traps. In this study, a myosin motor fleetingly grabs the actin filament suspended between the two optical trapped beads and strokes before letting go. (D) Optical traps can also be used to study the polymerization of biofilaments. Here a polymerizing microtubule is immobilized by attachment to two optically trapped beads. As the microtubule grows it rams against a glass pillar pushing against the optical forces.

change to the particle. The force on the particle at a particular displacement from the focus is linearly proportional to the total laser power – the more rays that are diffracted, the more force is imparted to the particle. The situation gets slightly more complicated when one considers the more realistic case of a Gaussian laser mode, one in which the intensity profile of the laser beam in a plane perpendicular to the direction of propagation is a two–dimensional Gaussian (Fig. 2B).

When the dielectric particle is very small compared to the wavelength of light it can be approximated as a perfect dipole that feels a Lorentz force due to the gradient in the electric field (Fig. 2C). Because the beam profile is Gaussian, the Lorentz force points towards the focus and is equal to

$$\boldsymbol{F} = (\boldsymbol{p} \cdot \bigtriangledown)\, \boldsymbol{E} + \frac{1}{c}\frac{d\boldsymbol{p}}{dt} \times \boldsymbol{B} \tag{1}$$

where $\boldsymbol{p} = \alpha \boldsymbol{E}$ is the dipole field and α is the polarizability. Optical traps are typically used with a continuous wave (CW) laser such that $\frac{\partial}{\partial t}\,(\boldsymbol{E} \times \boldsymbol{B}) = 0$. In this case the time-averaged force becomes

$$\langle \boldsymbol{F} \rangle = \frac{\alpha}{2} \bigtriangledown \langle \boldsymbol{E^2} \rangle \tag{2}$$

Typically, optical trapping experiments are performed using 500–nm polystyrene or glass spheres and a 1064–nm wavelength trapping laser. This combination of bead size and laser wavelength puts the real physics somewhere between the ray–optic and dipole regimes. The full theory of Mie scattering can get quite complicated, but the intuition gained from the other representations shown in Figure 2 remains useful even if it is not completely accurate.

A restoring force also exists in the axial dimension. If the particle is displaced axially below the laser focus (Fig. 3A), the overall direction of the laser propagation is not changed, but the divergence is. Rays

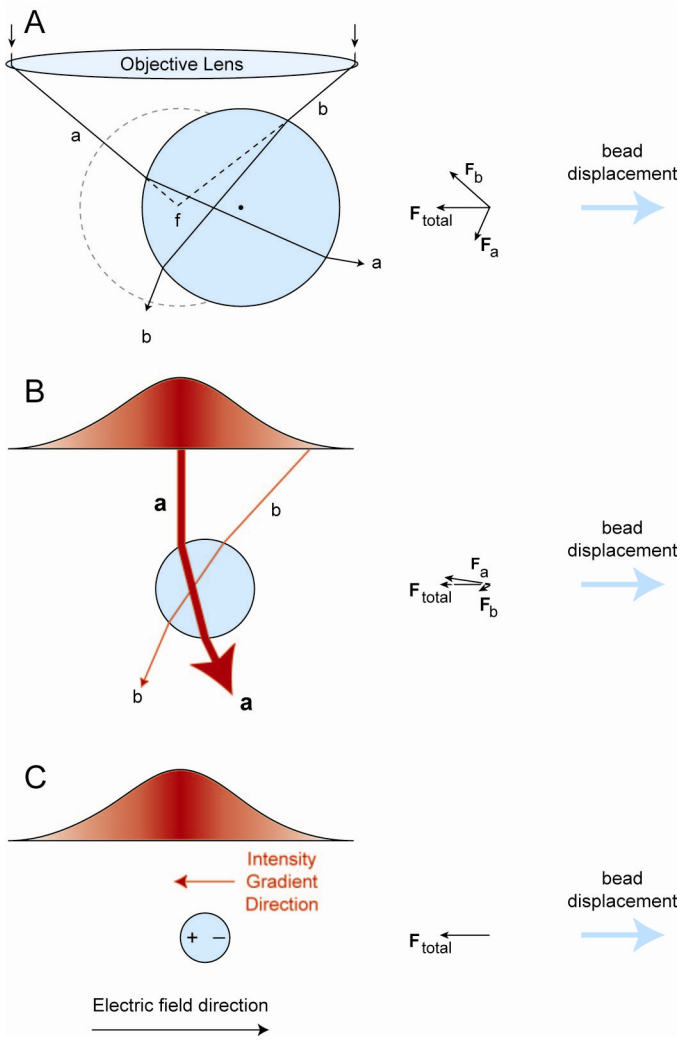

Figure 2: Simplified illustrations of optical trapping. (A) The simplest ray-optics diagram. In the absence of the bead, two rays (a and b) are focused through the objective lens to position f, the true laser focus. Refraction through the bead, which is displaced to the right of the laser focus, causes the new focus to lie to the right of f. After exiting the bead, ray a is bent up and to the right of its original trajectory, while ray b is deflected down and to the right. $\boldsymbol{F_a}$ and $\boldsymbol{F_b}$ represent the forces imparted to the bead by rays a and b; $\boldsymbol{F_{total}}$ is the sum of these two vectors and points to the left. (B) The force from a single-beam gradient optical trap with Gaussian intensity profile; two rays are drawn. The central ray, a, is of higher intensity than the extreme ray, b. Again, the bead is displaced to the right of the true laser focus. The total force on the bead, $\boldsymbol{F_{total}}$, again points to the left. (C) Dielectric particles much smaller than the wavelength of light can be considered to be perfect dipoles. The gradient in intensity, and hence electric field, produces a Lorentz force on the particle directed towards the laser focus.

a and b are refracted such that the new focus within the bead lies below f, and are more convergent upon exiting the bead. This slight refocusing of the laser causes a force on the particle pointing upwards, towards the laser focus f. The opposite is true when the particle is above the focus and the rays become more divergent (Fig. 3B).

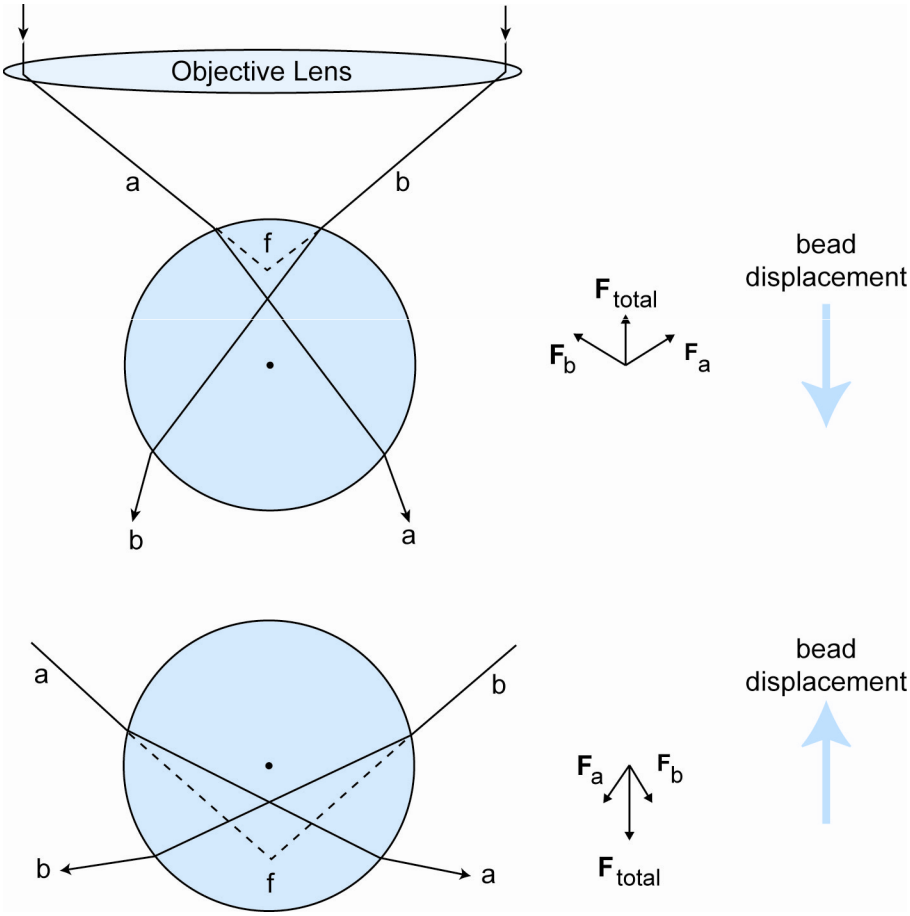

Figure 3: Description of axial trapping forces. Axial displacements of a bead in an optical trap change the relative amount of divergence of the focused laser light. In the absence of the bead, two rays (a and b) are focused through the objective lens to position f, the true laser focus. (A) Refraction through the bead, which is displaced below the laser focus, causes the new focus to lie below f. Upon exiting the bead the two rays are more convergent; ray a is bent down and to the left, while ray b is deflected down and to the right. $\boldsymbol{F_a}$ and $\boldsymbol{F_b}$ represent the forces imparted to the bead by rays a and b; $\boldsymbol{F_{total}}$ is the sum of these two vectors and points to upwards. (B) When the bead is displaced above the laser focus, the deflected rays a and b are more divergent, and the resulting force points downward.

Not all of the light is refracted through the particle; some gets reflected backwards. The force associated with these rays, the scattering force, pushes the particle away from the laser focus and causes the center of the optical trap to exist at a position displaced axially from the focus.

3 Microscope basics

As described in the previous section, all that is needed to make an optical trap is a laser and a lens. In practice however the lens must be a high numerical aperture, multi–element lens and the system must be capable of handling standard microscope slides. For these reasons, most optical trapping instruments are modifications of commercial microscopes [38], although some groups build them from scratch [47]. A collimated laser sent into the objective lens is focused to a diffraction–limited spot in the image plane forming the optical trap. It is important that the direction of laser propagation be parallel to the objective lens axis such that the optical trapping axes are aligned with the microscope axes. The objective and condenser lenses are set up in a telescope by imaging the field iris in the image plane of the microscope (Fig. 4). This telescope will become important later in the discussion of back-focal plane detection and beam steering. Koehler illumination, achieved by imaging the lamp filament in the plane of the condenser iris with a Bertrand lens, results in a very uniform field of illumination in the image plane and allows for excellent differential–interference microscopy. Two excellent texts on microscopy techniques are Inoue and Spring [17] and Murphy[29].

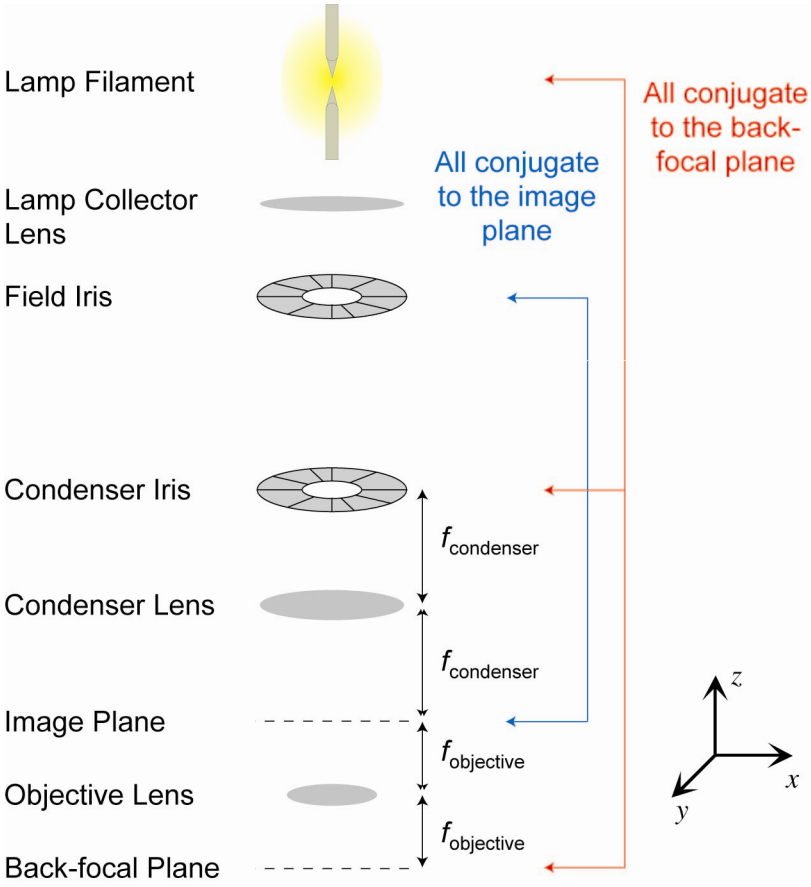

Figure 4: Microscope diagram with Koehler Illumination. In Koehler illumination two sets of conjugate planes are created using the lamp collector, condenser and objective lenses. The lamp filament, condenser iris, and objective back-focal plane are all in conjugate positions, as are the field iris and image plane. The lateral dimensions, x and y, and axial dimension, z, are all defined relative to the optical axis.

In a typical experiment, a sample of proteins, beads, and buffer is loaded onto a flow cell made by attaching a KOH–cleaned coverslip to a standard microscope slide with double–sided tape. Two pieces of tape are mounted such that the space between them forms a channel through which fluid can be added on one end and extracted on the other (Fig. 5). The thickness of the flow cell is about 40 μm.

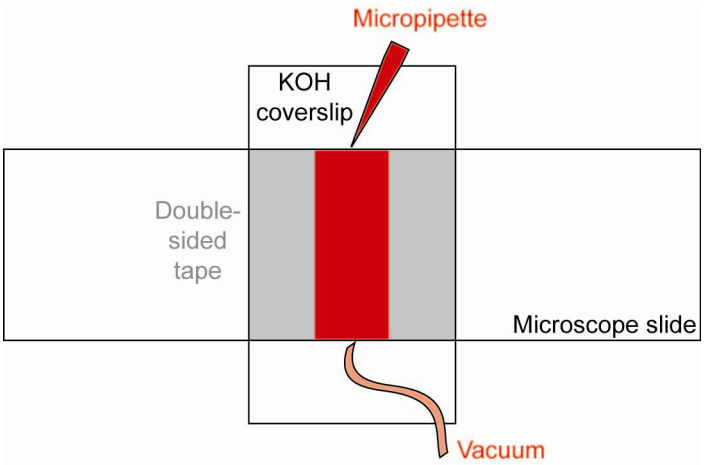

Figure 5: Flow cell construction. A KOH-cleaned coverslip is attached to a standard microscope slide by two pieces of double–sided tape (grey) forming a central channel. Fluid can be flowed through this channel with a micropipette and extracted from the other wide by applying a small vacuum. The flow-cell is mounted coverslip–side down on the microscope to avoid spherical aberrations that arise when imaging through the much thicker slide.

4 Lens basics

The basic properties of a thin lens are displayed in Figure 6. Parallel rays get focused to a single spot one focal distance away (Fig. 6A). This property allows one to use a lens to create an image of object on the other side of the lens (Fig. 6B). The thin lens equation (3) relates the distances to the image and the object to the focal distance.

$$\frac{1}{i} + \frac{1}{o} = \frac{1}{f} \tag{3}$$

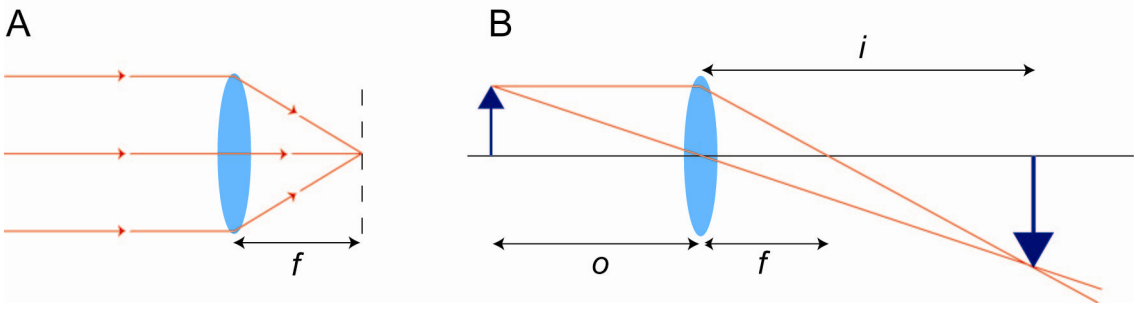

Figure 6: Basic lens properties. A lens is a curved material used to change the convergence of light rays. (A) Parallel rays impingent on a lens become focused at a distance equal to the focal length of the lens, f. (B) A lens can be used to create an image. The distance to the object, o, and image, i, are related to the focal distance by Equation (3).

Two lenses can be combined to form a Keplerian telescope by separating them by the sum of their focal lengths (Fig. 7). In this configuration, collimated light coming in remains collimated after the

telescope. Telescopes can be used to change the diameter of a collimated laser beam (Fig. 7B), but are also useful for propagating conjugate planes for the purpose of beam steering (see below).

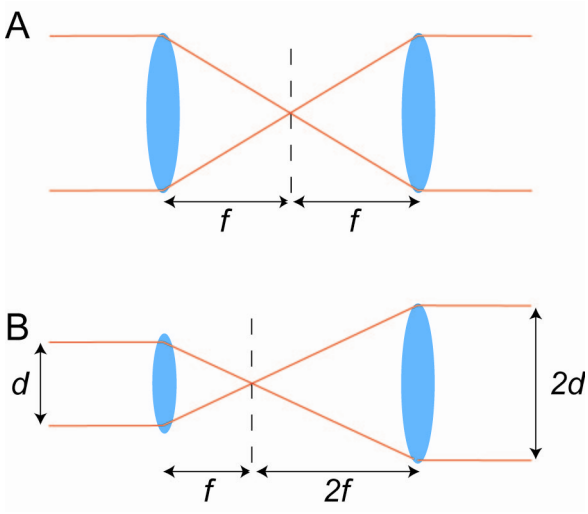

Figure 7: Telescopes can be formed with two lenses. A Keplerian telescope is formed by separating two lens by the sum of their focal lengths. The magnification of the telescope is equal to the second focal length divided by the first. Assuming the light is traveling from left to right, a 1:1 (A) and a 2:1 (B) telescope are shown.

Telescopes can also be used as laser beam collimators. By changing the spacing between two lenses, a collimated beam can be made to be convergent or divergent, and visa–versa. This control will be useful for changing the axial position of the optical trap. An example using a one–to–one telescopic collimator is shown in Figure 8.

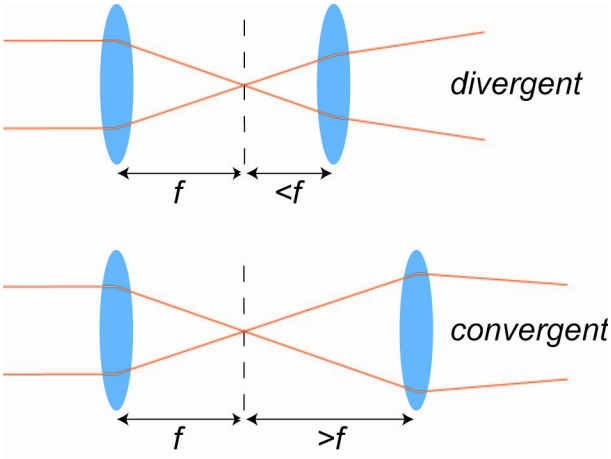

Figure 8: Telescopes can change the divergence of a laser beam. By placing the lens closer than the sum of the two focal lengths, a telescope can make the impingent light more divergent. If the lens are a larger distance apart, the beam becomes more convergent.

5 Beam steering

Beam steering in an optical trap is achieved by rotating the direction of laser beam propagation in a plane conjugate to the back focal plane of the objective (Fig. 9).

The back–aperture of the objective is usually inside the microscope housing so that it is not practical to place optical elements there for the purposes of beam steering. Instead, relay imaging using telescopes can be used to transmit rotations from a conjugate plane to the back- aperture. This method preserves the collimation of the trapping laser at the same time as producing translations of a well aligned optical

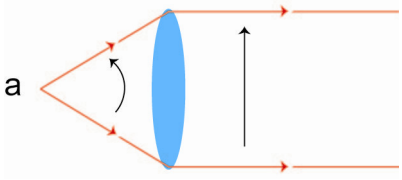

Figure 9: Lenses turn rotations into translations. Rotations at position a, one focal length behind the lens, become translations after the lens.

trap. Figure 10 demonstrates how rotations can be propagated with relay imaging. Rotations at a are imaged into rotations at c, which would presumably be the back-aperture of the microscope objective. Because the two lenses are set up in a telescope, the collimation of the laser at c is the same as at a. With a one–to–one telescope (Fig. 10A) rotations at a are the same magnitude as at c, whereas fora one–to–two telescope, rotations at a are reduced by a factor of two (Fig. 10B).

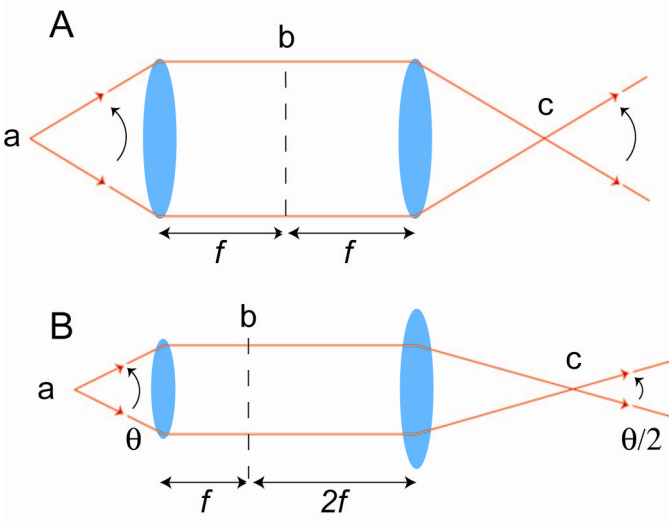

Figure 10: Rotations can be propagated with relay imaging. Relay image with a telescope propagates rotations along the beam path between conjugate planes without changing the laser beam collimation. Rotations at position a in a 1:1 telescope (A) produce rotations of the same magnitude at c, whereas the rotations are reduced by a factor of two in a 2:1 telescope (B).

Rotations need not be created exactly one focal distance behind the lens of a telescope. For any arbitrary Keplerian telescope with focal lengths f_1 and f_2 (Fig. 11), rotations at a distance x behind the first lens, position a, are recreated at a distance y after the telescope, position c, where y is given by

$$y = f_2 - \left(\frac{f_2}{f_1}\right)^2 (x - f_1) \tag{4}$$

The magnitude of the rotation at c is equal to f_1/f_2 times the magnitude at a.

Although mirrors are the most obvious choice for producing rotations of the trapping beam, lenses can also be used. As diagramed in Figure 12, translation of the lens at position a rotates the laser beam. By putting this lens into a telescope, rotations can be achieved at b while keeping the laser beam collimated. The distance to b is given by $i = (f_1 + f_2)\, f_2/f_1$.

Slight adjustment of the collimation of the trapping beam can be used to change the axial position of an optical trap relative to the image plane (Fig. 13). Similar to the situation presented in Figure 8,

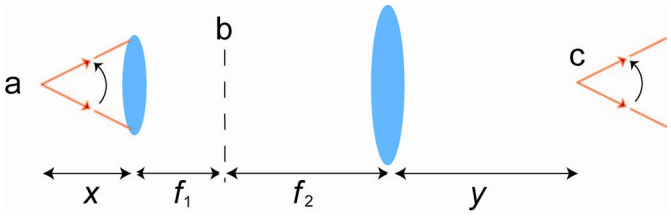

Figure 11: Position of conjugate planes relative to a telescope. The Keplerian telescope creates a conjugate plane to a at position c. The distance y can be found from x and the two focal lengths using Equation (4).

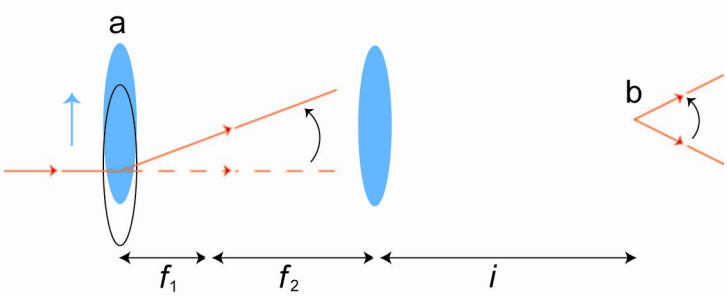

Figure 12: Translation of a lens causes rotations of the trapping laser. Translation of the lens a yields a rotation of the impingent laser beam. By placing this lens in a telescope, the rotations at a are imaged onto a conjugate plane at b a distance i from the second lens.

adjustment of the axial position of lens a in Figure 12 produces changes in the collimation of the trapping laser. Therefore, the optical trap can be steered in three dimensions using a single lens.

6 Acousto-optic deflectors

Rotations can also be produced using an acousto–optic deflector (AOD), a high optical–density crystal in which a traveling sound wave creates a moving diffraction pattern. In an AOD, a piezo–electric transducer is coupled to a diffracting crystal, usually made of TeO_2 for 1064–nm trapping light, which is angle cut at the opposite end and fixed to an acoustic absorber (Fig. 14). The transducer is driven with an RF drive signal of 10 V pk–to–pk at a frequency of about 30 MHz generated by a PCI–bus, computer-controlled frequency generator and amplified with an RF amplifier. The induced sound wave propagates through the crystal, creating traveling regions of high and low material, and hence optical, density. A laser beam input at roughly the Bragg angle diffracts off this moving grating with most of the power in the first-order diffracted beam. Adjustment of the frequency of the sound wave manifests as a change in the spacing of the diffraction grating, because the speed of sound in the crystal is fixed. Therefore, changes in the deflection angle of the first-order diffracted beam are linearly proportional to changes in the frequency of the RF drive signal

$$\Delta\theta_{deflection} \approx \lambda \frac{\Delta f}{V_{sound}} \tag{5}$$

where λ is the wavelength of light in air and V_{sound} is the speed of sound in the crystal. The angular position of the diffracted beam can be changed very quickly by adjustment of the drive frequency with

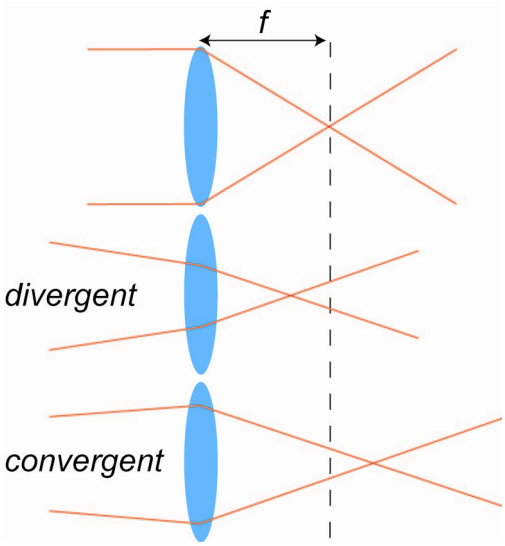

Figure 13: Adjustment of the axial position of an optical trap. Adjustment of the collimation of the input laser changes the position of the focus relative to the image plane (dashed line).

a fast, computer–controlled RF generator. This time response is limited only by the time required for the traveling wave to cross the laser beam, and so is equal to the laser beam diameter divided by the acoustic speed, about 5 μs for a 3 mm beam. AODs are especially useful because they are inherently random access. Unlike lenses or mirrors, one need not sweep though a series of intermediate angles when changing from one position to another.

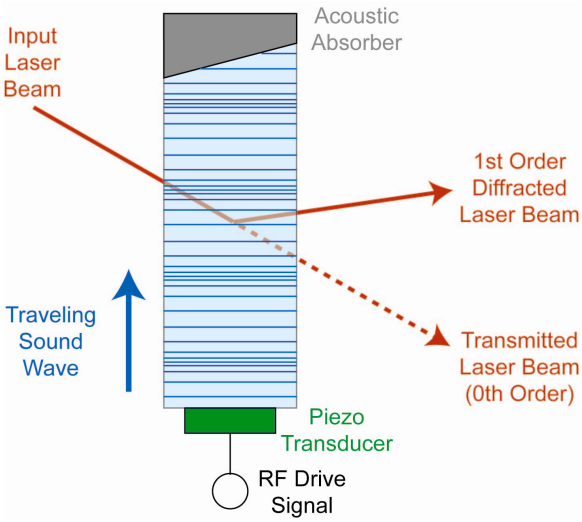

Figure 14: Schematic of an acousto-optic deflector. A 10 V RF sine wave drives the piezo–electric transducer (green) which is mechanically coupled to the AO crystal (light blue). This creates a traveling sound wave with period regions of high and low material density (dark blue). The end of the AO crystal is angle cut and attached to an acoustic absorber (grey). Laser light (red) diffracts off the diffraction grating created by the sound wave. Changes in the frequency of the sound wave cause proportional changes in the angle of the 1st order diffracted beam.

The absorber on an AO crystal does not absorb all the acoustic energy, and reflections off the back surface interfere with the main traveling wave and set up acoustic standing waves. This interference has two effects. Firstly, the response time to changes in angular deflection is increased to as much as 100 μs as a new standing wave pattern is created. Secondly, interactions of the laser light with the standing

wave cause nonlinearities in the deflection angle, so that Equation (5) holds only approximately. These nonlinearities are on the order of 5–10 μrad from the nominal value, which typically translates into 5 nm uncertainty in the position of the optical trap (Fig. 15).

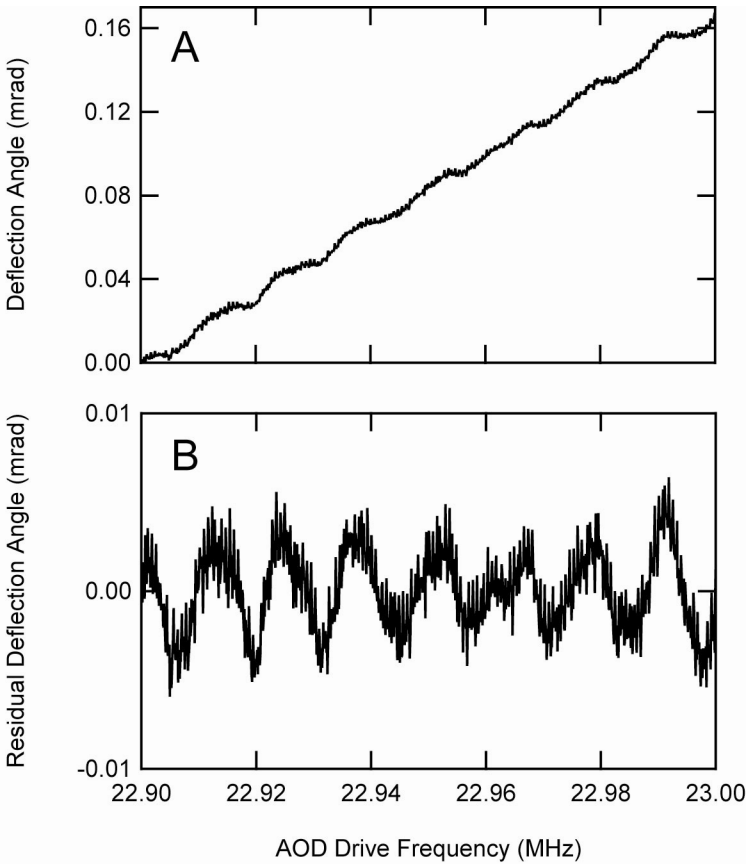

Figure 15: Nonlinearity in the AOD angular deflection. (A) The angular deflection of one AOD crystal as a function of the driving frequency. Nonlinearities in the response are due to standing waves created in the AO crystal. (B) Residual from a line fit to the data in A.

In addition to altering beam angle, AODs can be used to change the intensity and frequency of the first-order diffracted beam. Changes in the amplitude of the RF driving signal alter the efficiency of the diffraction and can be used to modulate the intensity of the first-order beam. Because the sound wave is moving in the crystal, the frequency of the first-order diffracted light is Doppler shifted. As drawn in Figure 14, the sound wave fronts are moving towards the incident laser light and hence the diffracted light is up-shifted in frequency. A pair of AODs, aligned orthogonally, can be used to deflect the trapping laser beam in two-dimensions. By placing these crystals in a plane conjugate to the back–focal plane of the objective, one can control the position of an optical trap in the image plane in two–dimensions (for example at position a in Figure11). Typically, both lens steering, for coarse positioning, and AODs, for fine computer control of trap position, are designed into an optical trapping apparatus as shown in Figure 16. With a 3:1 total beam expansion after a pair of IntraAction Corp. TeO_2 AOD crystals going into a Nikon 100× 1.4 N.A. objective, a frequency change of 1 MHz, corresponding to an angular change of 1.7 mrad, moves the optical trap by about 1.1 μm. The instrument diagram in [24] incorporates all

the elements shown in Figure 16.

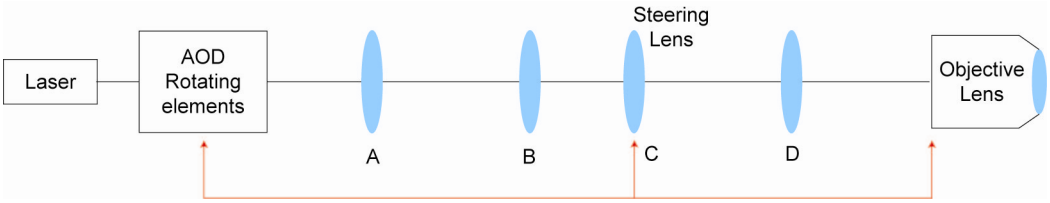

Figure 16: Typical optical trapping setup with steering lens and AODs. Lenses A and B, and C and D are setup in Keplerian telescopes. Lens D creates an image of the back-focal plane onto lens C, which can be used to steer the optical trap both laterally and axially. Telescope AB creates an image of lens C, and hence the back–focal plane, onto the AODs, which are used to steer the optical trap laterally.

The alignment of a pair of acousto–optic deflectors is often difficult. One requires that the diffraction efficiency be high, 60-80% through each crystal, and that this efficiency be as uniform as possible across the range of angles used, 17 mrad or 10 MHz. In practice, aligning the AODs is as much an art as a science, and the best geometry is often found by trial and error. An example of the diffraction efficiency through a pair of IntraAction AODs is shown in Figure 17.

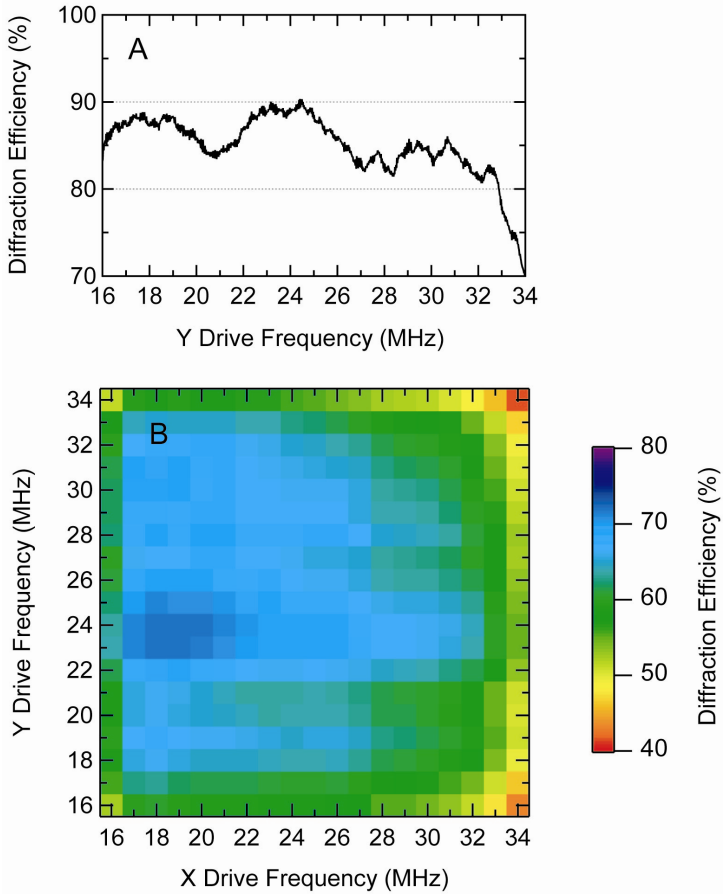

Figure 17: The diffraction efficiency of a pair of AODs. (A) The diffraction efficiency of a single crystal as a function of RF driving frequency. The efficiency is very high on average, 85%, but shows significant variation with changes in frequency. (B) In a pair of AODs, the 1st order diffracted beam from the first crystal moves slightly over the face of the second crystal causing further modulations in the total diffraction efficiency. The average efficiency of this pair of crystals is 63%.

7 Position detection

Modern optical traps use a separate detection laser to monitor the position of a trapped or stuck bead. A separate laser allows one to maximize the total range, and sensitivity of bead detection, as well as allowing for on-the-fly calibrations of a trapped bead [24]. As shown in Figure 2, lateral displacements of a bead near the focus of a laser cause rotations in the direction of laser propagation. These rotations occur in the image plane where the laser is focused, and hence cause translations in the back-aperture of the condenser. Recall that the objective and condenser lenses are set up in a Keplerian telescope when aligning Koehler illumination. Like the objective, the back-aperture of the condenser lens is inaccessible in a microscope, and so a lens is used to image a photodetector into a plane conjugate to the back–focal plane (Fig. 18). Translations of a bead in the laser focus cause translations of the detection laser in the back-focal plane and are detected either by a quadrant photodiode (QPD) [24], or more recently, a position sensitive detector (PSD) [35], which are able to record the position of the center–of–intensity of the laser light in two dimensions.

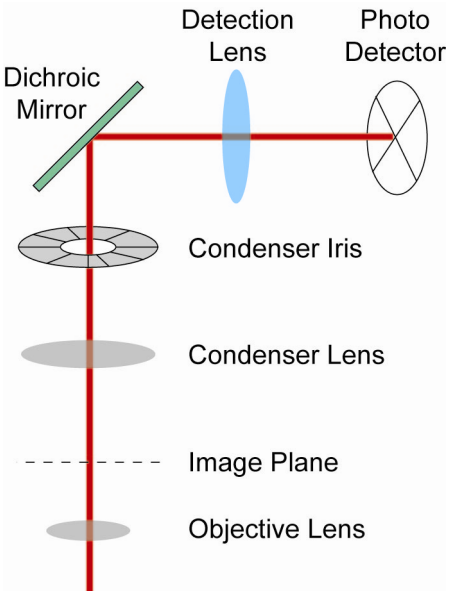

Figure 18: Diagram of back-focal plane detection. The detection lens is positioned such that the back–focal plane of the condenser is imaged onto a 2D photodetector. Rotations of the detection laser (red) cause translations in the back–focal plane which are read out at the detector. A dichroic mirror (green) is reflects the detection laser (usually either red or infrared), but transmits the green light used for imaging.

Axial motions can also be detected using an optical trap. Figure 3 demonstrates that axial displacements of a bead through a laser focus change the collimation of the laser. As the detection laser light passes through the condenser iris, the outer–most ring of light is blocked from the detector. When a bead moves through the laser focus axially, the relative amount of light that is blocked changes, and so the total amount of light impingent on the photodetector also changes. There is a trade off between the lateral and axial detection sensitivities. Because the axial detection relies on blockage of the outer edges of the detection beam, narrowing the condenser iris, effectively reducing the condenser numerical aperture, increases sensitivity to axial motions. In contrast, the lateral detection scheme monitors the rotation of the laser light in the image plane, which has a large contribution from the outer most rays. The diameter of the condenser iris is usually set such that the lateral and axial detection sensitivities fit the needs of the experiment at hand. The position detector is calibrated by moving a trapped or stuck bead while monitoring the x–, y–, and z–voltage signals from the photodetector. A detailed description of this procedure can be found in Lang et al. [24] and Pralle et al. [31].

8 Trap stiffness determination

For small motions of a bead near the center of an optical trap, the forces acting on the bead approximate a zero rest–length, linear spring at the trapping center. Recall this position is offset from the laser focus due to the scattering force. Considerable effort has been placed on measuring the trap stiffness with high accuracy. Many methods have been developed for this purpose, three of which will be described in detail here.

The easiest of these methods calculates the variance in the Brownian motion of a trapped bead. By the equipartition theorem, the energy in the Brownian motion of the trapped bead is equal to $\frac{1}{2}k_BT$, whereas the energy stored in the spring is equal to the one half times the spring constant, α, times the variance in the motion. Setting these two energies equal and solving for the stiffness yields

$$\alpha = \frac{\langle x^2 \rangle}{k_B T} \tag{6}$$

Calculation of the variance in position is straightforward, and is an easy way to estimate the trap stiffness although one needs a calibrated position detector.

The most useful method involves measuring the frequency spectrum of the Brownian noise exhibited by the bead. Typically, the mass of the bead is so small that the Reynolds number is very low and inertial forces are much weaker than those of hydrodynamic drag. In this regime, the equation of motion for the bead is that of a massless, damped oscillator driven by Brownian motion

$$\beta \dot{x}(t) + \alpha x(t) = F(t) \tag{7}$$

where x is the position of the bead, $\beta = 6\pi\eta r$ is the drag coefficient of the bead, η is the viscosity of the surrounding fluid, and r is the bead radius. The Brownian noise source, $F(t)$, has zero mean, and is essentially white with amplitude

$$\left|\tilde{F}(f)\right|^2 = 4\beta k_B T \tag{8}$$

The Fourier transform of Equation (8) is

$$2\pi\beta\left(\frac{\alpha}{2\pi\beta} - if\right)\tilde{x}(f) = \tilde{F}(f) \tag{9}$$

The power spectrum is then given by

$$|\tilde{x}(f)|^2 = \frac{k_B T}{\pi^2 \beta\left[\left(\frac{\alpha}{2\pi\beta}\right)^2 + f^2\right]} \tag{10}$$

Equation (10) is that of a Lorentzian with corner frequency $f_c = \alpha/2\pi\beta$. Therefore the stiffness of the trap is given by $\alpha = 2\pi\beta f_c$. Power spectra measurement and subsequent fitting of the corner frequency are easily achieved and usually take a few seconds. Typical trap stiffnesses of 0.1 pN/nm yield a corner frequency of around 3 kHz for a 500–nm bead. If the trapping center is relatively close to the focus of the detection laser beam then the position to photodetector voltage calibration will be linear and the corner frequency can be found from the power spectrum of the voltage data.

Optical traps typically work around one micron above the coverslip, where the hydrodynamic drag coefficient of the bead is altered by the proximity of the surface. The viscous drag on a sphere of radius r whose center is a distance h above a surface is

$$\beta = \frac{6\pi\eta r}{1 - \frac{9}{16}\left(\frac{r}{h}\right) + \frac{1}{8}\left(\frac{r}{h}\right)^3 - \frac{45}{256}\left(\frac{r}{h}\right)^4 - \frac{1}{16}\left(\frac{r}{h}\right)^5} \tag{11}$$

A useful table of correction values can be found in [38]. The height of the bead above the coverslip surface can be found by monitoring the axial detection signal as the surface is moving into contact with the bead [24].

In addition to the corner frequency, the power spectra contains information about the overall frequency response of the detection system. Unintended filtering, caused by a weak response of the photodetector to the infrared detection laser, or poorly designed electronics, will cause the high frequency portion of the power spectrum to fall below that of a true Lorentzian and reduce the apparent stiffness (for a very complete analysis see [5]). Extra noise may be caused by poor mounting of an optic or the clipping of the detection laser on something which vibrates. These vibrations can be seen at relatively low frequencies in the power spectrum. Extra noise in the position signal causes the measured stiffness to be too low, whereas unintended filtering emulates a stiffer trap due to the relative reduction in total noise. The variance method described above allows for none of these problems to be diagnosed.

To better understand the effect of filtering on a power spectral analysis of trap stiffness consider Figure 20, which shows the power spectra for two trapped beads with the same drag coefficient, but where one trap is 10 times stiffer than the other. You can see that at the higher stiffness the total ampitude is lower, but also that more relative information is contained at higher frequencies.

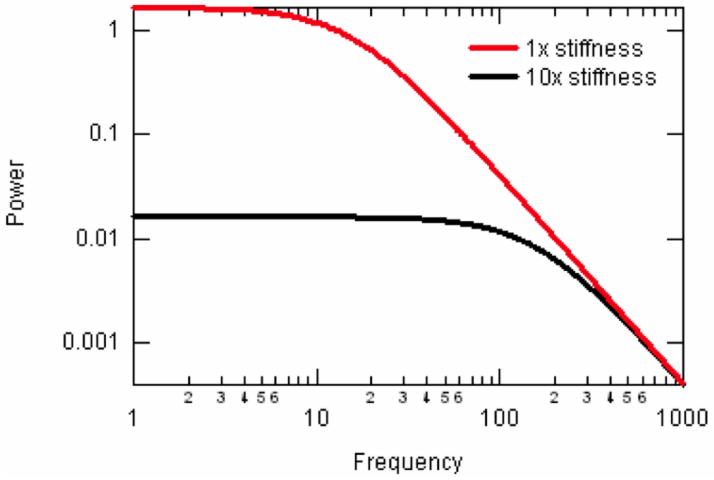

Figure 19: Calculated power spectrum for two trapped beads, with one trap 10 times stiffer than the other.

The variance calculation is essentially an integration of the power spectra over the aquisition frequency range. Figure 19 shows the relative error, i.e. the integral of the power spectrum up to maximum frequency divided by the actual variance (zero is bad and one perfect). For the weaker trap the integral quickly converges to the correct answer, but for the stronger trap you have to integrate out to a much higher frequency. With a limited bandwidth, lets say 200 in the units of Figure 19, you get just about the right answer for the weaker trap stiffness, but would be 65% too high for the stronger trap using the variance method.

A third method of stiffness calibration directly balances the trapping force with a drag force. The coverslip, attached to a piezo-controlled microscope stage, is moved at a constant velocity. Forces up 10 pN on a 500–nm bead can be achieved by moving the stage at a velocity of 2 mm/s, close to the limit of the current generation of nanopositioning stages. For a given velocity, the trap stiffness is given by

$$\alpha = \frac{\beta v}{\Delta x} \tag{12}$$

where β is the drag coefficient corrected for the proximity to the surface, v is the stage velocity and Δx is the measured displacement of the bead from the trap center. By measuring the displacement for a

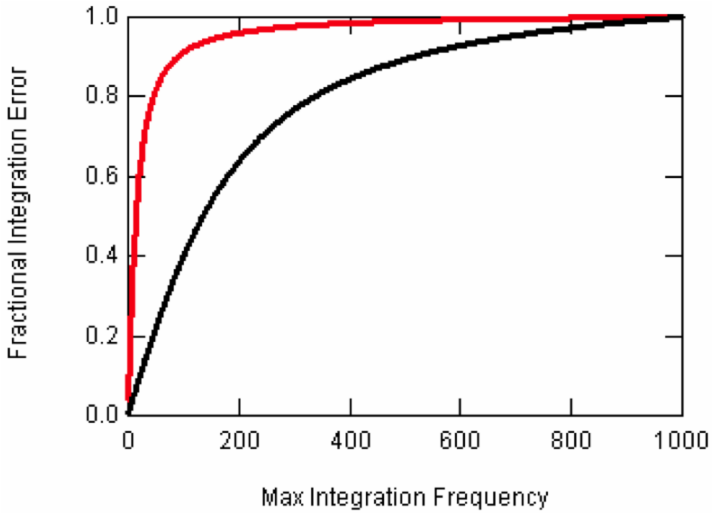

Figure 20: Fractional error when calculating the variance at a limited bandwidth.

series of different stage velocities, one is able to use this method to probe the linearity of the optical trap, something that cannot be done with the other two methods. In practice, this calibration method is less straight forward than the others. The stage z–axis is never exactly aligned with the optical axis of the microscope such that large lateral movements change the relative height of the bead above the coverslip. This is accounted for by measuring the slope of the surface height change and compensating for this during the sweep. In addition, the PI stages takes tens of milliseconds to get up to the desired speed. Considering that the total range of the stage is 100 μm laterally, a 2 mm/s sweep lasts for only 50 ms. Care must be taken to only sample the bead displacement when the stage is at the desired speed. When all extra sources of noise and filtering are taken into account, the three different methods of calibrating trap stiffness usually agree to within 5–10%. It is a good idea to use all three methods when first calibrating an optical trap. However, on a daily basis, the power- spectrum method affords the most information in the least amount of time.

9 Computer control and optical traps

Much effort has been spent designing optical traps so that they may be controlled via a computer. Not only does this make many things easier through the use of large programs that combine many complicated tasks, but it also allows for software feedback to be used where hardware algorithms would be difficult to implement [24]. Currently, computer control of the Physik Instrumente microscope stage is via a GPIB interface, although a higher speed method is now available using a National Instruments PXI interface. These stages have capacitive position feedback with an accuracy of 0.3 nm and a range of $100\times100\times20\mu$m. The AOD drive frequency is generated by a PCI-bus card which is run with custom software from IntraAction Corp. These cards are accessed directly via specific memory addresses in the case of the Windows 95/98 operating systems with an access time of 10 μs on a 500 MHz Pentium III Dell computer, or by going through the central kernel in a Windows NT system with an access time of 20 μs on a 2 GHz Pentium 4 Dell computer. Data from the QPD or PSD are processed by custom electronics [24, 35], and anti–alias filtered before A/D conversion by a National Instruments DAQ board. Real–time video from a CCD camera placed in the image plane of the microscope is digitized with a National Instruments PCI card. This video signal can be used to track the position of a bead in three dimensions, with some limitations. Software to control the stage, and AODs, as well as to sample the position detection signals is written in National Instruments LabVIEW. LabVIEW interfaces extremely

well with the National Instruments hardware described above, and makes it easy to create graphical user interfaces. Currently, data analysis software is written in Wavemetrics Igor Pro, which offers a good blend of numerical programming and presentation-ready graphics.

References

[1] M. W. Allersma, F. Gittes, M. J. deCastro, R. J. Stewart, and C. F. Schmidt. Two-dimensional tracking of ncd motility by back focal plane interferometry. *Biophys J*, 74(2 Pt 1):1074–85., 1998.

[2] A. Ashkin. History of optical trapping and manipulation of small-neutral particel, atoms, and molecules. *IEEE Journal of Selected Topics in Quantum Electronics*, 6(6):841–856, 2000.

[3] A. Ashkin, J. M. Dziedzic, and T. Yamane. Optical trapping and manipulation of single cells using infrared laser beams. *Nature*, 330(6150):769–771, 1987.

[4] A. Ashkin, J.M. Dziedzic, J.E. Bjorkholm, and S. Chu. Observation of a single-beam gradient force optical trap for dielectric particles. *Optics Letters*, 11(5):288, 1986.

[5] Kirstine Berg-Sorensen, Lene Oddershede, Ernst-Ludwig Florin, and Henrik Flyvbjerg. Unintended filtering in a typical photodiode detection system for optical tweezers. *Journal of Applied Physics*, 93(6):3167–3176, 2003.

[6] S. M. Block. Making light work with optical tweezers. *Nature*, 360(6403):493–5, 1992.

[7] S. M. Block. Nanometres and piconewtons: the macromolecular mechanics of kinesin. *Trends in Cell Biology*, 5:169–175, 1995.

[8] S. M. Block, D. F. Blair, and H. C. Berg. Compliance of bacterial flagella measured with optical tweezers. *Nature*, 338(6215):514–8, 1989.

[9] S. M. Block, L. S. Goldstein, and B. J. Schnapp. Bead movement by single kinesin molecules studied with optical tweezers. *Nature*, 348(6299):348–52., 1990.

[10] C. Bouchiat, M. D. Wang, J. Allemand, T. Strick, S. M. Block, and V. Croquette. Estimating the persistence length of a worm-like chain molecule from force-extension measurements. *Biophys J*, 76(1 Pt 1):409–13, 1999.

[11] C. M. Coppin, D. W. Pierce, L. Hsu, and R. D. Vale. The load dependence of kinesin's mechanical cycle. *Proc Natl Acad Sci U S A*, 94(16):8539–44., 1997.

[12] I. Crevel, N. Carter, M. Schliwa, and R. Cross. Coupled chemical and mechanical reaction steps in a processive neurospora kinesin. *Embo J*, 18(21):5863–72., 1999.

[13] R. J. Davenport, G. J. Wuite, R. Landick, and C. Bustamante. Single-molecule study of transcriptional pausing and arrest by e. coli rna polymerase. *Science*, 287(5462):2497–500, 2000.

[14] J. T. Finer, R. M. Simmons, and J. A. Spudich. Single myosin molecule mechanics: piconewton forces and nanometre steps. *Nature*, 368(6467):113–9., 1994.

[15] N. R. Forde, D. Izhaky, G. R. Woodcock, G. J. Wuite, and C. Bustamante. Using mechanical force to probe the mechanism of pausing and arrest during continuous elongation by escherichia coli rna polymerase. *Proc Natl Acad Sci U S A*, 99(18):11682–7, 2002.

[16] Y Harada, O Ohara, A Takatsuki, H Itoh, N Shimamoto, and K Kinosita. Direct observation of dna rotation during transcription by escherichia coli rna polymerase. *Nature*, 409(6816):113–5, Jan 2001.

[17] S. Inoue and K. Spring. *Video Microscopy: The Fundamentals*. Plenum Press, New York, 1997.

[18] S Kasas, NH Thomson, BL Smith, HG Hansma, X Zhu, M Guthold, C Bustamante, ET Kool, M Kashlev, and PK Hansma. Escherichia coli rna polymerase activity observed using atomic force microscopy. *Biochemistry*, 36(3):461–8, Jan 1997.

[19] K. Kawaguchi and S. Ishiwata. Temperature dependence of force, velocity, and processivity of single kinesin molecules. *Biochem Biophys Res Commun*, 272(3):895–9, 2000.

[20] K. Kawaguchi and S. Ishiwata. Nucleotide-dependent single- to double-headed binding of kinesin. *Science*, 291(5504):667–9., 2001.

[21] J. W. J. Kerssemakers, M. E. Janson, A. van der Horst, and M. Dogterom. Optical trap setup for measuring microtubule pushing forces. *Applied Physics Letters*, 83(21):4441–4443, 2003.

[22] S. C. Kuo. Using optics to measure biological forces and mechanics. *Traffic*, 2(11):757–63, 2001.

[23] M. J. Lang and Steven M. Block. Resource letter: Lbot-1: Laser-based optical tweezers. *American Journal of Physics*, 71(3):201–215, 2003.

[24] M.J. Lang, C.L. Asbury, J.W. Shaevitz, and S.M. Block. An automated two-dimensional optical force clamp for single molecule studies. *Biophys J*, 83(1):491–501, Jul 2002.

[25] R. Mallik, B. C. Carter, S. A. Lex, S. J. King, and S. P. Gross. Cytoplasmic dynein functions as a gear in response to load. *Nature*, 427(6975):649–52, 2004.

[26] R Mallik, D Petrov, SA Lex, SJ King, and SP Gross. Building complexity: an in vitro study of cytoplasmic dynein with in vivo implications. *Curr Biol*, 15(23):2075–85, Dec 2005.

[27] J. E. Molloy. Optical chopsticks: digital synthesis of multiple optical traps. *Methods in Cell Biology*, 55:205–16, 1998.

[28] J. E. Molloy, J. E. Burns, J. Kendrick-Jones, R. T. Tregear, and D. C. White. Movement and force produced by a single myosin head. *Nature*, 378(6553):209–12., 1995.

[29] D.B. Murphy. *Fundamentals of Light Microscopy and Electronic Imaging*. Wiley-Liss Inc., 2001.

[30] KC Neuman, EA Abbondanzieri, R Landick, J Gelles, and SM Block. Ubiquitous transcriptional pausing is independent of rna polymerase backtracking. *Cell*, 115(4):437–47, Nov 2003.

[31] A. Pralle, M. Prummer, E. L. Florin, E. H. Stelzer, and J. K. Horber. Three-dimensional high-resolution particle tracking for optical tweezers by forward scattered light. *Microsc Res Tech*, 44(5):378–86., 1999.

[32] M. Rief, R. S. Rock, A. D. Mehta, M. S. Mooseker, R. E. Cheney, and J. A. Spudich. Myosin-v stepping kinetics: a molecular model for processivity. *Proc Natl Acad Sci U S A*, 97(17):9482–6., 2000.

[33] R. S. Rock, S. E. Rice, A. L. Wells, T. J. Purcell, J. A. Spudich, and H. L. Sweeney. Myosin vi is a processive motor with a large step size. *Proc Natl Acad Sci U S A*, 98(24):13655–9, 2001.

[34] A. Rohrbach and E. H. K. Stelzer. Trapping forces, force constants, and potential depths for dielectric spheres in the presence of spherical aberrations. *APPLIED OPTICS*, 41(13):2494–2507, May 2002.

[35] JW Shaevitz, EA Abbondanzieri, R Landick, and SM Block. Backtracking by single rna polymerase molecules observed at near-base-pair resolution. *Nature*, 426(6967):684–7, Dec 2003.

[36] GM Skinner, CG Baumann, DM Quinn, JE Molloy, and JG Hoggett. Promoter binding, initiation, and elongation by bacteriophage t7 rna polymerase. a single-molecule view of the transcription cycle. *J Biol Chem*, 279(5):3239–44, Jan 2004.

[37] S.P. Smith, S.R. Bhalotra, A.L. Brody, B.L. Brown, E.K. Boyda, and M. Prentiss. Inexpensive optical tweezers for undergraduate laboratories. *Am. J. Phys.*, 67(1):26–35, 1998.

[38] K. Svoboda and S. M. Block. Biological applications of optical forces. *Annu Rev Biophys Biomol Struct*, 23:247–85, 1994.

[39] K. Svoboda, C. F. Schmidt, D. Branton, and S. M. Block. Conformation and elasticity of the isolated red blood cell membrane skeleton. *Biophys J*, 63(3):784–93, 1992.

[40] K. Svoboda, C. F. Schmidt, B. J. Schnapp, and S. M. Block. Direct observation of kinesin stepping by optical trapping interferometry. *Nature*, 365(6448):721–7., 1993.

[41] C. Veigel, L. M. Coluccio, J. D. Jontes, J. C. Sparrow, R. A. Milligan, and J. E. Molloy. The motor protein myosin-i produces its working stroke in two steps. *Nature*, 398(6727):530–3, 1999.

[42] C. Veigel, F. Wang, M. L. Bartoo, J. R. Sellers, and J. E. Molloy. The gated gait of the processive molecular motor, myosin v. *Nat Cell Biol*, 4(1):59–65, 2002.

[43] K. Visscher and S. M. Block. Versatile optical traps with feedback control. *Methods Enzymol*, 298:460–89, 1998.

[44] K. Visscher, M. J. Schnitzer, and S. M. Block. Single kinesin molecules studied with a molecular force clamp. *Nature*, 400(6740):184–9., 1999.

[45] M. D. Wang, M. J. Schnitzer, H. Yin, R. Landick, J. Gelles, and S. M. Block. Force and velocity measured for single molecules of rna polymerase. *Science*, 282(5390):902–7., 1998.

[46] M. D. Wang, H. Yin, R. Landick, J. Gelles, and S. M. Block. Stretching dna with optical tweezers. *Biophys J*, 72(3):1335–46, 1997.

[47] GJ Wuite, RJ Davenport, A Rappaport, and C Bustamante. An integrated laser trap/flow control video microscope for the study of single biomolecules. *Biophys J*, 79(2):1155–67, Aug 2000.

[48] R. Yasuda, H. Noji, Jr. Kinosita, K., and M. Yoshida. F1-atpase is a highly efficient molecular motor that rotates with discrete 120 degree steps. *Cell*, 93(7):1117–24, 1998.